Biochimica et Biophysica Acta 1828 (2013) 1013–1024

Contents lists available at SciVerse ScienceDirect

Biochimica et Biophysica Acta

journal homepage: www.elsevier.com/locate/bbamem

Membrane thickness and the mechanism of action of the short peptaibol trichogin GA IV

S. Bobone [a], Y. Gerelli [b], M. De Zotti [c], G. Bocchinfuso [a], A. Farrotti [a], B. Orioni [a], F. Sebastiani [b], E. Latter [d], J. Penfold [d], R. Senesi [e,f], F. Formaggio [c], A. Palleschi [a], C. Toniolo [c], G. Fragneto [b], L. Stella [a,*]

[a] University of Rome "Tor Vergata", Department of Chemical Sciences and Technologies, 00133 Rome, Italy
[b] Institut Laue-Langevin (ILL), 38000-Grenoble, France
[c] ICB, Padova Unit, CNR, Department of Chemistry, University of Padova, 35131 Padova, Italy
[d] ISIS, STFC, Rutherford Appleton Laboratory, Chilton, Didcot, OXON, OX11 0QX, UK
[e] University of Rome "Tor Vergata", Department of Physics and Centro NAST, 00133-Rome, Italy
[f] CNR-IPCF, Italy

ARTICLE INFO

Article history:
Received 25 September 2012
Received in revised form 20 November 2012
Accepted 27 November 2012
Available online 5 December 2012

Keywords:
Membrane thickness
Molecular dynamics simulations
Neutron reflectivity
Peptaibiotics
Peptide embedding in a bilayer
Transmembrane peptides

ABSTRACT

Trichogin GA IV (GAIV) is an antimicrobial peptide of the peptaibol family, like the extensively studied alamethicin (Alm). GAIV acts by perturbing membrane permeability. Previous data have shown that pore formation is related to GAIV aggregation and insertion in the hydrophobic core of the membrane. This behavior is similar to that of Alm and in agreement with a barrel-stave mechanism, in which transmembrane oriented peptides aggregate to form a channel. However, while the 19-amino acid long Alm has a length comparable to the membrane thickness, GAIV comprises only 10 amino acids, and its helix is about half the normal bilayer thickness. Here, we report the results of neutron reflectivity measurements, showing that GAIV inserts in the hydrophobic region of the membrane, causing a significant thinning of the bilayer. Molecular dynamics simulations of GAIV/membrane systems were also performed. For these studies we developed a novel approach for constructing the initial configuration, by embedding the short peptide in the hydrophobic core of the bilayer. These calculations indicated that in the transmembrane orientation GAIV interacts strongly with the polar phospholipid headgroups, drawing them towards its N- and C-termini, inducing membrane thinning and becoming able to span the bilayer. Finally, vesicle leakage experiments demonstrated that GAIV activity is significantly higher with thinner membranes, becoming similar to that of Alm when the bilayer thickness is comparable to its size. Overall, these data indicate that a barrel-stave mechanism of pore formation might be possible for GAIV and for similarly short peptaibols despite their relatively small size.

1. Introduction

Antimicrobial peptides (AMPs) are produced by all organisms as a first defense against pathogens. They exhibit multiple roles, including chemotactic and immunomodulatory functions [1], but their main activity is bactericidal, often through the perturbation of the permeability of bacterial membranes [2]. This mechanism of action makes the development of bacterial resistance particularly unlikely. It is for this reason that AMPs are investigated as a possible solution to the dramatic health problem of multiple drug-resistant bacteria [3]. However, in order to develop new molecules with the same activity as AMPs, but with better drug-like properties [4,5], it is essential to understand their mechanism of pore formation in detail.

Most AMPs are cationic [6] and perturb membrane permeability according to the Shai–Matsuzaki–Huang (SMH) model [7–10]. They bind to the membrane surface, parallel to it, thus modifying its surface tension and eventually leading to the formation of local bilayer defects that allow the passage of hydrophilic and charged molecules.

Another class of pore-forming, bactericidal peptides, which was actually discovered well before cationic AMPs, is represented by peptaibols, or peptaibiotics [11]. These peptides are produced non-ribosomally by fungi, are characterized by a C-terminal 1,2-amino alcohol and a high content of non proteinogenic residues, most notably α-aminoisobutyric acid (Aib), and are usually acetylated or acylated at the N-terminus. Peptaibiotics are usually helical both in solution and when membrane-

Abbreviations: HFIP, 1,1,1,3,3,3-hexafluoroisopropanol; Aib, α-aminoisobutyric acid; Alm, alamethicin; AMP, antimicrobial peptide; CF, carboxyfluorescein; DIEA, N,N-diisopropylethylamine; DMF, N,N-dimethylformamide; EDC, N-ethyl, N′-[3-(dimethylamino)propyl]carbodiimide; Fmoc, fluorenyl-9-methyloxycarbonyl; GAIV, trichogin GAIV; HATU, O-(7-azabenzotriazol-1-yl)-1,1,3,3 tetramethyluronium hexafluoro phosphate; HOAt, 7-aza-1-hydroxy-benzotriazole; Lol, leucinol; MD, molecular dynamics; *n*Oct, *n*-octanoyl; POPC, 1-palmitoyl-2-oleoyl-*sn*-glycero-3-phosphocholine; SLD, scattering length density; SMH, Shai–Matsuzaki–Huang

* Corresponding author at: Dipartimento di Scienze e Tecnologie Chimiche, Università di Roma "Tor Vergata", via della Ricerca Scientifica 1, 00133 Rome, Italy. Tel.: +39 06 7259 4463; fax: +39 06 7259 4328.
E-mail address: stella@stc.uniroma2.it (L. Stella).

0005-2736/$ – see front matter © 2012 Elsevier B.V. All rights reserved.
http://dx.doi.org/10.1016/j.bbamem.2012.11.033

bound, and, unlike cationic AMPs, their content of charged residues is very low or even absent altogether. The best characterized member of this family (and the second to be identified, in 1967) is alamethicin (Alm) [12]. For this peptide it has been conclusively demonstrated through a combination of a large set of biophysical techniques that it forms pores through a mechanism different from the SMH model, and termed "barrel-stave" [13–20]. In this case, equilibria between different peptide alignments in the bilayer exist [21,22], but when the membrane-bound peptide concentration is sufficiently high and/or a transbilayer potential is applied, peptide helices insert in a transmembrane orientation and aggregate in a cylindrical superstructure, like the staves in a barrel, with the more hydrophilic side of the helices facing the water-filled channel lumen. This model was first proposed in 1974, but until now it has been convincingly demonstrated only for Alm.

Alm comprises 19 amino acids and its helix has a length corresponding almost exactly to the thickness of biological membranes (Fig. 1). However, it is also one of the longest members of the peptaibiotic family, which contains peptides going from 21 amino acids (SCH 643432) to just 4 (peptaibolin) [11]. Considering the closely related amino acid composition and physico-chemical properties of all members of the peptaibiotic family, it is conceivable that they could form pores in a similar way. However, an important drawback seems to preclude the formation of transmembrane pores to shorter peptides: how could such short helices form channels spanning through the whole bilayer?

A well characterized, medium-length peptaibiotic is trichogin GA IV (GAIV henceforth), whose sequence is *n*Oct-Aib^{1}-Gly^{2}-Leu^{3}-Aib^{4}-Gly^{5}-Gly^{6}-Leu^{7}-Aib^{8}-Gly^{9}-Ile^{10}-Lol, where *n*Oct is *n*-octanoyl, and Lol is leucinol [23]. This 10-mer peptide was isolated from *Trichoderma longibrachiatum* in 1992 [24] and since then it was studied both in solution and in model membranes by a number of physico-chemical techniques [25], including NMR [24,26], X-ray crystallography [27], EPR [28–33], fluorescence [34–40], electrochemistry [41,42], and molecular dynamics simulations [10]. Its 3D-structure is helical, with a flexible hinge in the central part, formed by two consecutive Gly residues [24,27,37,38]. In this conformation, its length is only about half the normal thickness of a biological membrane (Fig. 1). For this reason, different models were proposed to explain its pore-forming activity, including the SMH mechanism [26,28,43] and a carrier function [29,30]. However, several evidences would favor a barrel-stave structure for its pores, just like Alm. In this connection, by combining several different fluorescence experiments we showed that, above a threshold concentration, GAIV inserts deeply into the hydrophobic core of the membrane and forms aggregates. These inserted, aggregated species are responsible for membrane leakage [34–36]. Later on, these findings were confirmed by EPR measurements [31–33]. Other studies established that GAIV-induced membrane permeability is ion-selective and depends on the sign and magnitude of the transmembrane potential, exactly like that of Alm channels [41,42,44].

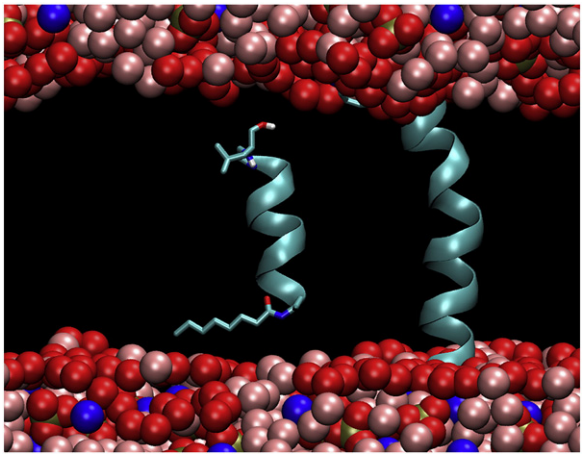

Fig. 1. Comparison of the length of the Alm and GAIV helices with the thickness of a POPC bilayer. Phosphorus, nitrogen and oxygen atoms of phospholipids are shown as gold, blue and red spheres, respectively, while water oxygen atoms are colored in pink. The acyl chains of the phospholipids are omitted for the sake of clarity. Peptides are represented as ribbons. The N-terminal acyl and C-terminal amino alcohol groups are shown in a "stick" representation. (For interpretation of the references to color in this figure legend, the reader is referred to the web version of this article.)

One hypothesis that was put forward to solve the apparent contradiction between these data and the short length of the GAIV helix is formation of head-to-head dimers able to span the entire bilayer [27,32]. However, this hypothesis seems not to be supported by the voltage dependence of GAIV-induced membrane permeability, which would require a co-linear alignment of the helices forming the channel, to generate an overall dipole that could sense the transbilayer potential [44].

In a previous study [10], we investigated GAIV location inside a lipid bilayer by molecular dynamics (MD) simulations using a self-assembling approach [45,46] that we defined as "minimum bias" [47,48]. In this method, the simulation starts from a random mixture of lipids and water, containing one peptide molecule. During the simulation, a lipid bilayer self-assembles spontaneously, but in the initially highly fluid environment the peptide is able to attain its most favorable position in the membrane. This study [10] indicated a possible solution to the problem of the mismatch between membrane thickness and peptide length. In two out of three such simulations with GAIV, the peptide positioned close to the membrane surface, parallel to it, without significantly perturbing the membrane. However, in a third simulation it inserted into the bilayer in a transmembrane orientation. This simulation showed a bilayer that, near the peptide, was significantly thinned, so that the short GAIV helix was able to span completely the membrane. Nevertheless, this preliminary result could not rule out the possibility that the observed effect was an artifact of the way the bilayer formed, since in this simulation GAIV was initially inserted in a local defect of the membrane, which healed only after an extensive simulation. The short length of the equilibrated segment of that simulation (10 ns) left open the possibility that the observed bilayer structure was just a transient, metastable state, which would eventually relax. More importantly, this purely computational but intriguing indication needed an experimental verification.

Here, we report combined experimental and simulative data supporting the possibility for GAIV to form barrel-stave channels. Neutron reflectivity studies were used to experimentally verify the effects of GAIV on bilayer thickness. Moreover, vesicle leakage experiments were exploited to determine the influence of membrane thickness on GAIV activity. In addition, our previous MD simulation studies were significantly extended, to confirm the stability of the transmembrane orientation, even when starting from a preformed bilayer, and to verify the cumulative effects of multiple membrane-inserted peptide chains. Overall, these data indicate that GAIV might be able to form barrel-stave channels by causing a significant thinning of the bilayer to a thickness comparable with the length of its helix.

2. Materials and methods

2.1. Materials

All phospholipids were purchased from Avanti Polar Lipids (Alabaster, AL, USA). Spectroscopic grade organic solvents were obtained from Carlo Erba Reagenti (Milano, Italy). Carboxyfluorescein (CF), Triton-X 100, and Sephadex-G50 were Sigma Aldrich (St. Louis, MO) products. Fmoc-Aib-OH (Fmoc, fluorenyl-9-methyloxycarbonyl) and Fmoc-Gly-OH were supplied from Novabiochem (Merck Biosciences, La Jolla, CA). N, N-dimethylformamide (DMF), N,N-diisopropylethylamine (DIEA), piperidine, N-methylmorpholine, 1,1,1,3,3,3-hexafluoroisopropanol (HFIP),

and Fmoc-OSu (1-oxy-succinimide) were purchased from Sigma-Aldrich (St. Louis, MO). N-Ethyl, N′-[3-(dimethylamino)propyl]carbodiimide (EDC), O-(7-azabenzotriazol-1-yl)-1,1,3,3 tetramethyluronium hexafluorophosphate (HATU), and 7-aza-1-hydroxy-benzotriazole (HOAt) were purchased from GLS (Shangai, China). *n*-Octanoic (*n*Oct) acid-d_{15}, L-leucine-d_{10}, and L-isoleucine-d_{10} were purchased from Euriso-top (Saint-Aubin, France).

2.2. Peptide synthesis and characterization

Native GAIV was synthesized as previously reported [49]. Fmoc-protection of deuterated residues was achieved by reaction with 1.2 equivalents of Fmoc-OSu and 1 equivalent of triethylamine in water/CH_3CN. Yield: 70%. A GAIV analogue deuterated on the Leu and Ile residues, and on *n-octanoyl*, was synthesized by manual solid phase peptide synthesis on a 0.05 mmol scale, starting with L-leucinol 2-chlorotrityl resin (Iris Biotech, Marktredwitz, Germany) (110 mg, loading 0.45 mmol g^{-1}). Fmoc-deprotection was performed with a 20% piperidine solution in DMF (reaction time: 5 min, repeated twice). The coupling steps, carried out in presence of HATU and DIEA, were doubled and followed by a capping protocol using acetic anhydride in a large excess. The *n*Oct moiety at the N-terminus was added by reaction with the preformed activated ester of *n*Oct-OH, obtained by reaction with an equivalent amount of EDC and HOAt in the presence of N-methylmorpholine. The 1-hour coupling procedure was repeated twice. Peptide cleavage from the resin was achieved by treatment with 30% HFIP in dichloromethane. The filtrate was collected and this step repeated three times (the last one was performed overnight). Then, the solution was concentrated under a flow of N_2. The crude peptide was purified by preparative HPLC on a Phenomenex C_{18} column (30×250 mm, particle size: 5 μm, pore size: 300 Å), using a Shimadzu (Kyoto, Japan) LC-8A pump system equipped with a SPD-6A UV-detector (flow rate 15 mL/min, λ = 216 nm) and a binary elution system: A, H_2O; B, CH_3CN/H_2O (9:1 *v/v*); gradient 40%–70% B in 30 min. The purified fraction was characterized by analytical RP-HPLC on a Vydac C_{18} column (4.6×250 mm, 5 μm, 300 Å) using a Dionex (Sunnyvale, CA) P680 HPLC pump with an ASI-100 automated sample injector. The binary elution system used was: A, 0.1% TFA (trifluoroacetic acid) in H_2O; B, 0.1% TFA in CH_3CN/H_2O (9:1 v/v); gradient 60%–80% B in 20 min (flow rate 1.5 mL min^{-1}); spectrophotometric detection at λ = 216 nm. Retention time: 14.3 min. Yield after purification: 50%. Purity > 97%. Electrospray ionization (ESI)-MS was performed on a PerSeptive Biosystem Mariner instrument (Framingham, MA). (*m/z*): calculated for $C_{52}H_{50}N_{11}O_{12}D_{45}$ $[M+H]^+$ 1112.01; found 1111.98.

2.3. Neutron Reflectometry (NR) experiments

Silicon single crystals (5×5×1 cm^3) cut along the (111) plane were cleaned by rinsing, under sonication, in chloroform, acetone, and ethanol. A 30 min UV/ozone treatment was used to make the polished surface more hydrophilic. Sample holders were laminar flow cells that allowed the injection of lipids and peptides and the exchange of the solvent to apply the well known contrast variation method [50]. To this aim, high purity D_2O (ILL) and Milli-Q water were used with the following ratios 1:0, 0:1 or 38:62 (for silicon-matched water or SMW) in order to obtain media with scattering length density (SLD or ρ) 6.35×10^{-6} $Å^{-2}$, -0.56×10^{-6} $Å^{-2}$ and 2.07×10^{-6} $Å^{-2}$, respectively. Neutron reflectivity experiments were performed at the silicon/water interface on the D17 reflectometer at ILL [51]. Specular neutron reflection gives information about the thickness and the compositional profile of a film along the direction normal to its surface (z). The overall process can be described by the classical theory of reflection of light, with a neutron refractive index $n \approx 1-\frac{\lambda_0^2\rho}{2\pi}$, where λ_0 is the incident wavelength and ρ the scattering length density. The latter parameter is directly related to the nuclear composition of the sample and changes upon isotopic substitution [52]. Neutron reflectivity data are measured as the ratio of intensities of the reflected and incident beams ($R = I/I_0$), as a function of the wave-vector transfer in the perpendicular direction to the layers interface Q_z. For a given incident wavelength λ_0 and angle α_i it is expressed as $Q_z = \frac{4\pi}{\lambda_0}\sin\alpha_i$. In our case, time-of-flight measurements were performed using wavelengths λ_0 in the range 2 to 18 Å together with two different angular configurations resulting in a covered Q_z going from 0.005 to 0.3 $Å^{-1}$.

Two silicon monocrystalline solid supports were used and characterized before the injection of lipid vesicles. Solid supported POPC (1-palmitoyl-2-oleoyl-*sn*-glycero-3-phosphocholine) and (d_{31})POPC lipid bilayers were obtained by the vesicle fusion method, which relies on spontaneous adhesion of the lipids to the surface following a vesicles spreading process [53]. Small unilamellar vesicles were formed by evaporating a chloroform lipid solution in a rotary vacuum system until a thin film was formed. Complete evaporation was ensured by applying a rotary vacuum pump for at least 2 h. Subsequently, the film was hydrated with phosphate buffer 10 mM, NaCl 140 mM, pH 7.4, for a final lipid concentration of 0.5 mg/mL. The vesicle suspension was sonicated by immersion of a titanium tip for three periods 10 min long at a power of 70 W, with suitable pauses between them to avoid excessive sample heating. Five milliliters of the vesicle suspension were injected in the sample flow cell. Excess of lipids not bound to the surface was removed by flushing water in the flow cell. To enhance the signal arising from the peptide molecules, addition of partially deuterated GAIV was used in combination with hydrogenated POPC, while hydrogenous peptides were added to the partially deuterated lipid bilayer. Four different concentrations of peptide were used, namely C_0 (bare lipid bilayer), C_1 (4.5 μM), C_2 (15 μM), and C_3 (30 μM). All of the peptide–lipids–solvent combinations exploited are reported in Table 1.

2.4. NR data analysis

The measured specular reflectivity data are connected to the arrangement of the material within the sample along the normal to the deposition interface. The relation can be summarized by the master formula [54]

$$R(Q_z) = \frac{16\pi^2}{Q_z^4}\left|\int \frac{d\rho(z)}{dz} e^{iQ_z z} dz\right|^2 \quad (1)$$

where the compositional information is described by the SLD along the z direction, $\rho(z)$.

A limitation in the analysis of NR data is the impossibility of a direct Fourier transform of the reflectivity $R(Q_z)$ that would result in the SLD profile, as evident from Eq. (1). This limitation, known as phase-loss problem, can be overcome using the contrast variation method, *i.e.* modeling data originated from the same sample with different isotopic substitutions. The more are the contrasts available, the higher is the accuracy in the data modeling. For example, in the present experiment, all of the data available for a given concentration (Table 1) were modeled simultaneously to exploit this peculiarity of NR.

The data fitting procedure was based on the Parratt's recursion relation [55], originally derived for reflection of X-rays but nowadays

Table 1
Available datasets.

Lipids	Peptide	Concentration	D_2O	SMW	H_2O
POPC	–	C_0	X	X	X
(d_{31})POPC	–	C_0	X	X	X
POPC	Deuterated	C_1	X		X
POPC	Deuterated	C_2	X	X	
POPC	Deuterated	C_3	X	X	
(d_{31})POPC	Hydrogenated	C_1	X		X
(d_{31})POPC	Hydrogenated	C_2	X	X	
(d_{31})POPC	Hydrogenated	C_3	X		X

widely used also for neutron scattering data. The simultaneous fit of the data was performed using an homemade software written in Matlab. The minimization routine was Fminuit, a χ^2 fitting program for Matlab based on the MINUIT minimization engine of the CERN program library [56]. The system was modeled as a stack of four layers, each of them described by a triplet of parameters [thickness t, $\rho(f_k)$ and interfacial roughness σ]. The parameter f_k is the volume fraction of the k component within the selected layer (Eq. (2)).

The first layer was used to describe the SiO_2 layer together with its hydration water. The sets of parameters, for both blocks, were obtained during the preliminary characterization of the bare silicon supports and kept fixed during the subsequent analysis. The remaining layers were respectively used to model: (*i*) the inner hydrophilic headgroup region, (*ii*) the hydrophobic tail region and (*iii*) the outer headgroup layer. All of the information available about the sample components was introduced in the model as constraints. These values are summarized in Table S1 of the supporting materials.

If the composition of a layer is not uniform, *i.e.* in presence of more than one component, the SLD representing the layer can be expressed as a linear combination of the SLDs of the components, where the weighting factors are the component volume fractions. In general, for the *i*-th layer the SLD was expressed as

$$\rho_i = f^i \rho_i^{\mathrm{dry}} + f_w^i \rho_w + f_p^i \rho_p^{\mathrm{dry}} \quad (2)$$

where f^i, $f_w{}^i$, and $f_p{}^i$ are respectively the volume fractions of the lipid, water, and peptide components in the *i*-th layer, and their sum is normalized to unity.

2.5. Set-up of MD simulations

The GAIV X-ray diffraction determined structure [27] was used as the initial peptide conformation. The initial lipid bilayer structure for the simulations was downloaded from http://moose.bio.ucalgary.ca/download.html [57], and comprised 128 POPC lipids (64 per leaflet) and 2460 water molecules. 3102 additional water molecules were then added, to enable larger distances between the periodic images of the lipid leaflets in the direction perpendicular to the lipid/water interface. This system was equilibrated for 5 ns and simulated for further 15 ns, for comparison with peptide-containing membranes. The equilibrated bilayer was taken as the starting point for the simulations in the presence of GAIV. In the bilayer we inserted 1, 4 or 8 GAIV molecules, following the protocol described in the next paragraph. For the systems with 4 and 8 peptides, three independent simulations were performed starting from the configurations reported in Fig. S1. In all cases, both possible helix orientations with respect to the bilayer normal were included, with the nearest neighbor peptide molecules oriented in an antiparallel arrangement. However, while in the simulations with 4 GAIV molecules the peptide helices were relatively close to each other and oriented with the hydrophilic regions facing each other, the simulations with 8 molecules started from a periodic arrangement, to reproduce a hexagonal lattice, with the peptides as far as possible and with the same azimuthal orientation (Fig. S1).

2.6. Protocol for peptide insertion in the membrane

To insert the GAIV molecules into the bilayer, we developed a novel method to create in the membrane cavities of shape and dimensions corresponding to those of the peptide. This protocol is based on a gradual switching of a repulsive potential in the positions to be occupied by the peptide atoms, in order to push the lipid chains out of that volume, taking advantage of their intrinsic flexibility. The peptide atoms (excluding hydrogens) were treated as isolated dummy atoms with the van der Waals properties of the CH_3 atom type in the *ffgmx* force-field [58], as implemented in GROMACS [59]. These dummies were inserted in the fully hydrated bilayer, in the position to be eventually occupied by the peptides, with all their interactions initially switched off. Their van der Waals potential was then gradually and continuously increased up to its force-field value during a 50 ps stochastic dynamics simulation, in which the dummy atoms were position restrained with a harmonic potential with a force constant of 10^5 KJ mol^{-1} nm^{-2}. Note that in principle the specific atom types could be used, rather than treating all heavy atoms as CH_3. However, considering that we had simply to create a cavity of appropriate dimension and form, the adopted procedure is adequate and definitively simpler. The van der Waals interactions were calculated by using a soft core potential, as implemented in GROMACS [60], with a switch function between 0.8 and 0.9 nm; the α scaling factor and the power for λ in the "soft-core" potential were 0.5 and 1, respectively. To carry out the stochastic dynamics simulation, we adapted a standard procedure, usually adopted for free-energy calculations [http://www.bevanlab.biochem.vt.edu/Pages/Personal/justin/gmx-tutorials/free_energy/Files/nvt.mdp]. With respect to the conditions reported on that site, we adopted a linear variation for the λ parameters ($\Delta\lambda = 10^{-5}$), reduced the time step to 0.5 fs, and introduced a semi-isotropic Berendsen pressure coupling [61], with a reference pressure of 1 atm and a coupling time constant of 5 ps. During these simulations the interaction between dummy atoms were turned off, and bond constraints were not used. All of the MD simulations were performed using the freely available GROMACS 4.0.7 software package, without further modifications [59]. An image of the cavity formation process is shown in Fig. S2. After cavity formation the correct peptide atoms were substituted for the dummy atoms, and the system was equilibrated by an energy-minimization step and a first 10 ns MD run with position-restraining on the peptides.

2.7. MD trajectories calculation and analysis

The systems were simulated for 100 ns, adopting the conditions previously described [10,47], except that in the present study semi-isotropic pressure coupling was used. Molecular graphics were obtained with the program VMD (Visual Molecular Dynamics) [62]. SLD profiles were calculated from the last 10 ns of the MD simulations, as follows: the density profile along the axis normal to the bilayer was calculated for each element of the system by using the *g_density* utility of the GROMACS package. These density values were multiplied by the coherent scattering length of the corresponding element [52], and then summed together to obtain the overall SLD. When multiple simulations were performed at the same peptide/lipid ratio, the SLD profiles were averaged over all available trajectories. These calculated SLD profiles cannot be compared directly to the experimental ones, since the latter have silicon on one side of the membrane, while in the simulations the bilayer faced a water phase on both sides. To overcome this issue, the experimental profiles were made symmetrical by reflecting the water-facing side with respect to the center of the hydrophobic region.

Order parameters for the for the C – C bonds of the palmitic chains were calculated with respect to the bilayer normal, according to standard definitions [10,59], on the last 10 ns of the trajectories.

2.8. Membrane-perturbing activity experiments

For CF leakage experiments, vesicles were prepared by dissolving the lipids in a 1:1 methanol–chloroform mixture, and evaporating the solvent in a rotary vacuum system and then applying a rotary vacuum pump for at least 2 h. Subsequently, the film was hydrated with a 30 mM CF solution, prepared in 10 mM phosphate buffer, pH 7.4, titrated with 85 mM NaOH to make CF water-soluble, and containing 80 mM NaCl to make it isotonic to the dilution buffer (phosphate buffer 10 mM, NaCl 140 mM, pH 7.4, 270 mOsm).

The peptide was added to a 200 μM solution of 200 nm CF loaded-liposomes, prepared with lipids of different tail lengths. The CF

fluorescence signal was followed at $\lambda_{exc} = 490$ nm and $\lambda_{em} = 520$ nm. The fraction of peptide-induced leakage was determined 20 min after peptide addition to the liposomes solution by following the increase in the fluorescence signal. The value corresponding to total leakage (for signal normalization) was obtained by adding 1 mM Triton X-100 [35].

3. Results

3.1. Neutron reflectivity experiments

In order to experimentally assess GAIV association with a lipid bilayer and its effects on membrane structure, we performed neutron reflectivity experiments on a planar POPC bilayer supported by a silicon crystal and submerged in a water phase, to which increasing GAIV concentrations were added. Deuterated peptide, lipids and water were used in appropriate combinations to increase the reflectivity contrast (Table 1). Data were analyzed globally (Section 2).

3.2. Bare substrates

Two different Si substrated were used for the POPC and (d_{31})POPC bilayers. Before membrane deposition, these substrates were characterized using three different water compositions (Table 1). For that used in combination with hydrogenated POPC, the dioxide layer was characterized by a thickness $t_{ox} = 15.8 \pm 0.1$ Å, a volume fraction of hydrating water $f_{ox} = 0.15 \pm 0.05$ and a roughness $\sigma = 2.2 \pm 0.2$ Å. The block used for supporting deuterated lipids was characterized by the parameters $t_{ox} = 15.5 \pm 0.1$ Å, $f_{ox} = 0.12 \pm 0.05$, and $\sigma = 2.4 \pm 0.3$ Å. These values were kept fixed during the modeling of the sample data.

3.3. Bare POPC bilayer

The simultaneous fits on all of the available datasets for a pure lipid bilayer are shown in Fig. S3. The parameters obtained are in complete agreement with those already reported in the literature [63]. In both cases, the parameters of the pure lipid bilayer were indicative of a symmetric bilayer, with a total thickness of 48 ± 3 Å. The inner and outer headgroup regions were 10 Å thick ($t_h = 10 \pm 1$ Å), with a volume fraction of water $f_h = 0.5 \pm 0.1$. The hydrophobic core of the bilayer was 28 Å thick ($2 \times t_t = 28 \pm 1$ Å) with no water penetration, which suggests an almost perfect coverage of the substrate surface [64]. The roughness of all interfaces was similar and close to 2 Å. From these values the SLD profiles along the normal of the bilayer were evaluated. They are represented in Fig. S3.

3.4. Peptide effects

The same approach was used for the samples where the peptide was injected (at concentrations C_1, C_2, and C_3 corresponding to 4.5, 15, and 30 μM, respectively). A qualitative assessment of the experimental data indicated already that structural modifications induced by the peptide were taking place in the lipid bilayer.

In Fig. 2 the curves of the POPC bilayer in D_2O at the different concentrations of deuterated peptide investigated are compared. Two main features are visible. From the pure lipid bilayer to the C_3 sample a decrease in reflectivity in the mid-Q region (0.05–0.15 $Å^{-1}$) is observed that could be interpreted as a change of contrast between the sample and the solvent. Indeed, according to Eq. (2), addition of deuterated peptide molecules into a hydrogenated bilayer would lead to a total SLD closer to that of D_2O. It has to be reminded that the contrast is the difference between the SLD of the sample and that of the medium. The lower is this value, the weaker is the reflectivity (or scattering) signal.

The second feature clearly visible is a shift of the main minimum of the profiles towards higher Q_z values. For the pure POPC bilayer it

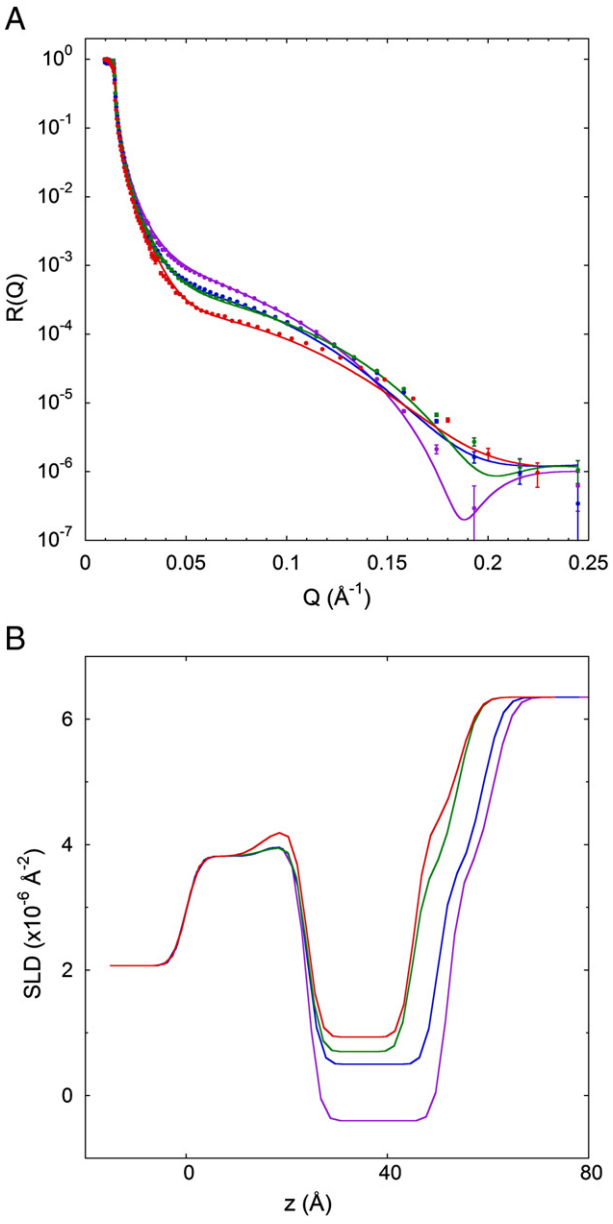

Fig. 2. A) Neutron reflectivity profiles for the POPC bilayer in D_2O, in the absence of GAIV (violet), and after addition of deuterated GAIV, at concentrations C_1 (blue), C_2 (green) and C_3 (red). B) Neutron scattering length density (SLD) profiles for the POPC-based samples at different deuterated peptide concentrations in D_2O (the color code is the same as that in panel A). The thinning of the hydrophobic region upon peptide addition is clearly visible. Also the increase of the amount of the included peptide within this region is indicated by the increase in the scattering length density between 25 Å and 45 Å. (For interpretation of the references to color in this figure legend, the reader is referred to the web version of this article.)

was located around $Q_z = 0.20$ $Å^{-1}$ and it shifted to higher values after peptide insertion. This is a clear indication of thinning of the overall thickness of the deposition.

From the simultaneous fits according to the Parrat's recursive formula, the sample at the four different peptide concentrations was characterized in a clear and unambiguous way. The resulting parameters are listed in Table 2. From these parameters we were able to determine the main structural changes induced by the peptide inclusion into the lipid bilayer. First of all, the peptide is present only in the hydrophobic layer, as described by the volume fractions f_{ph} and f_{pt}, representing the volume fraction of peptide molecules occurring in the headgroup and tail regions, respectively. f_{ph} is zero for all of the investigated samples. Instead, the quantity of peptide inserting into

Table 2
Parameters obtained from the fits of the data of the lipid–peptide systems at the four concentrations.

	C_0	C_1	C_2	C_3
t_h (Å)	10 ± 1	9 ± 1	8 ± 1	9 ± 1
$2\times t_t$ (Å)	28 ± 1	26 ± 1	23 ± 1	21 ± 1
f_h	0.5 ± 0.1	0.4 ± 0.1	0.4 ± 0.1	0.4 ± 0.1
f_t	0.00 ± 0.05	0.00 ± 0.05	0.05 ± 0.05	0.05 ± 0.05
σ_h *inner* (Å)	2 ± 1	2 ± 1	2 ± 1	2 ± 1
σ_h *outer* (Å)	2 ± 1	2 ± 1	2 ± 1	2 ± 1
σ_t (Å)	2 ± 1	2 ± 1	2 ± 1	2 ± 1
f_{ph}	n.a.	0	0	0
f_{pt}	n.a.	0.09 ± 0.02	0.11 ± 0.03	0.13 ± 0.05
N_{pt}/N_l	n.a.	0.07 ± 0.02	0.09 ± 0.02	0.10 ± 0.04

the hydrophobic layer is clearly concentration dependent. From the peptide volume fraction f_{pt}, and from the molecular volumes of GAIV and of the lipid tails we could evaluate the inserted peptide to lipid ratio at the different concentrations (N_{pt}/N_l), which goes from 7% at C_1 to 10% at C_3. Unfortunately, within the experimental accuracy, it was not possible to distinguish whether the peptide molecules are located in a specific part of the tail region or with a specific orientation with respect to the bilayer normal *z*.

The second important information arising from the modeling is that the inclusion of the peptide produces a thinning of the bilayer, especially because of a thickness decrease of the tail region. Actually, within the experimental accuracy, the headgroup thickness t_h is stable at all concentrations, while a decrease is observed in the t_t parameter (t_t is the thickness of the hydrophobic region of a single leaflet). The overall hydrophobic region is "compressed" by ~7 Å going from the pure lipid system to that with the highest amount of peptide included. This thinning affects the overall bilayer thickness, decreasing form 48 ± 3 Å to 39 ± 3 Å (Fig. 3). All of these structural changes are detectable also from a comparison of the SLD profiles, as shown in Fig. 2.

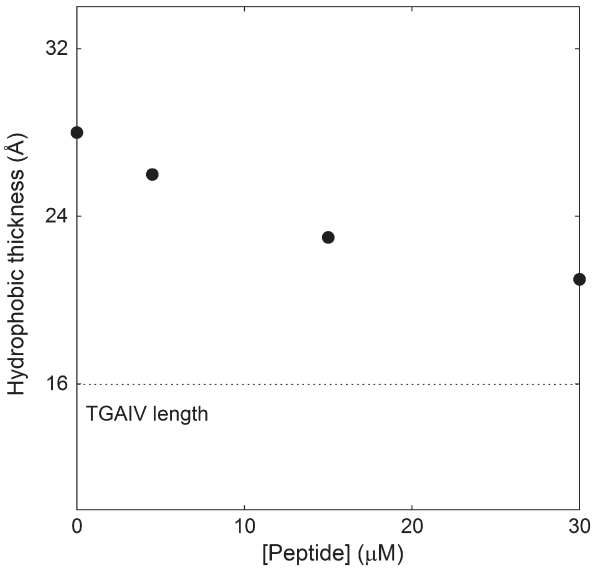

Fig. 3. Decrease in the thickness of the hydrophobic region of the bilayer caused by the addition of increasing GAIV concentration, as determined by the neutron reflectivity experiments. For comparison, the length of a GAIV helix is shown as a horizontal dotted line.

3.5. MD simulations

In order to understand at the molecular level the structural changes observed in the bilayer in the NR experiments, we performed MD simulations of GAIV-membrane systems. In a previous computational study [10] we showed that when GAIV is associated to the membrane parallel to its surface it does not cause any significant bilayer perturbation. Therefore, in the present study we investigated the stability of a transmembrane peptide orientation and its effects on the bilayer.

3.6. Protocol for peptide insertion in the membrane

Due to the shortness of the trichogin chain, we devised a novel approach for peptide insertion in a pre-equilibrated membrane. Previously reported methods of peptide/protein insertion in a membrane involve bilayer assembly around the molecule either by packing the lipids one by one, or by initially placing the lipids on a widely spaced grid and then 'shrinking' the grid until the bilayer has the desired density [65–67]. Other approaches involve formation of a pore that spans the entire bilayer either by removing some lipids and/or by using a repulsive potential [66–69]. However, when the molecule to be inserted is significantly shorter than the bilayer thickness (like GAIV) and is to be placed in the hydrophobic core of the membrane, these approaches would initially leave a part of the hydrophobic region of the bilayer exposed to water, *i.e.* a significantly unstable and unrealistic situation, and would require considerable equilibration times.

To avoid these problems, we developed a way to create a peptide-shaped cavity in the hydrophobic core of the membrane: peptide molecules were inserted in the middle of the bilayer, with all their interactions initially switched off. Their van der Waals potential was then gradually increased, up to the values of the simulation force field (see Section 2 for a detailed description of the procedure). In this way, cavities were formed, since the lipid chains were pushed out of the volume occupied by the peptide molecules (Fig. S2).

Other methods were previously reported to form a protein-shaped cavity similarly to our technique, but using more sophisticated approaches [70,71]. However, these methods often require manual intervention, because they involve several input parameters and no standard setting works for every system [72]. In addition, all of the methods presently available encounter further difficulties in cases where many copies of the same (small) molecule have to be inserted at different positions in the bilayer. For this kind of targets, the method presented here seems to be more suitable. In addition, since it does not require any specific software nor modification of complex codes, it is definitely simpler.

3.7. MD trajectories

After GAIV insertion in these cavities and an appropriate 10 ns equilibration period (during which the peptide was position-restrained), these simulations were continued for 100 ns more. We performed a total of 7 simulations: in one of them, only one peptide molecule was inserted in the bilayer (comprising 128 POPC lipid molecules), in three other simulations 4 GAIV molecules were inserted, and in further three simulations the peptides in the bilayer were 8 (see Fig. S3, and Section 2).

In most cases, the GAIV molecules maintained a transmembrane orientation for the whole trajectory, and quickly (*i.e.* in about 10–30 ns) some lipid headgroups in the region above and below the peptide were drawn deeper in the membrane, due to the interaction with the free peptide NH and CO groups at the two termini of the helices. A few structures representative of the time-evolution of the simulations are shown in Fig. 4, while the kinetics of peptide-induced bilayer thinning is reported in Fig. S4, and the structures at the end of the simulations are illustrated in Fig. 5.

To better define the interactions responsible for the observed bilayer deformation, we performed an analysis of the interactions of the peptide NH and CO groups not involved in intramolecular H-bonds, and of the OH group of the C-terminal amino alcohol, with

different parts of the lipid molecules or with water. This analysis was limited to the trajectory segment following the formation of the bilayer thinning, *i.e.* from 30 ns onward (Fig. 6). As expected, the NH groups at the N-terminus interact mainly with the oxygen atoms of the phosphate and glycerol groups, while the C-terminal CO groups were almost invariably associated with the quaternary ammonium of the lipid choline group. The OH group of Lol interacts mostly with the glycerol moiety. All three GAIV groups (NH, CO and OH) also interact with water molecules. These data indicate that the bilayer deformation is driven by electrostatic and H-bonding interactions, which are enhanced in the low-dielectric constant environment of the hydrophobic membrane core. These interactions lead to thinning by drawing phospholipid headgroups deep into the membrane, thus inducing an increase in the number of gauche conformations in the lipid tails, as shown by a progressive decrease in their order parameters, as the number of peptides in the bilayer increases (Fig. S5).

To further confirm the stability of the transmembrane state, we extended by further 40 ns the simulation previously obtained by using the "minimum bias approach", whose equilibrated segment was initially just 10 ns long. During this time, no significant modification in the peptide location, nor in the bilayer structure in its surroundings was observed (data not shown). The same system was simulated at 350 K for 65 ns without any evidence of destabilization of the transmembrane conformation.

Overall, these simulation strongly support the possibility of a transmembrane orientation for GAIV and a significant thinning effect on the bilayer, so that the short peptide helix could span it from one side to the other. However, it is important to note the limitations inherent in these computational results, which are mainly associated to the relatively short time scale that can be simulated. For instance, membrane-inserted GAIV molecules do not associate during our trajectories, while previously reported experiments indicate that this phenomenon does take place [31,33–35]. The lack of aggregation in the simulations is most likely due to the slow lateral diffusion of both lipids and peptides with respect to the length of the trajectories. We also know from experiments that the surface-bound state is highly favored for a monomeric GAIV molecule [35]. By contrast, the membrane inserted peptides essentially maintain the initial transmembrane orientation in most of the simulations, although some of the peptides move towards the bilayer surface in some of the trajectories with eight GAIV molecules. Once more, this is likely due to the limited length of the trajectories. Therefore, the present MD calculations are biased by the initial conditions, in which the peptides were placed in a monomeric, membrane-inserted transbilayer orientation. As such, they cannot rule out by themselves the formation of dimers with one GAIV molecule on top of the other to match the length of the bilayer, as proposed by some authors [27,32]. However, the spontaneous formation of a system with a transbilayer inserted GAIV monomer in one of the self-assembly simulations previously reported [10], and the stability of this orientation in all the calculations presented here, definitely indicate that this state, accompanied by membrane thinning, represents at least a local minimum in the free-energy surface. In any case, a comparison of the MD trajectories with the experimental neutron data can be used to assess the reliability of the picture provided by the computational results.

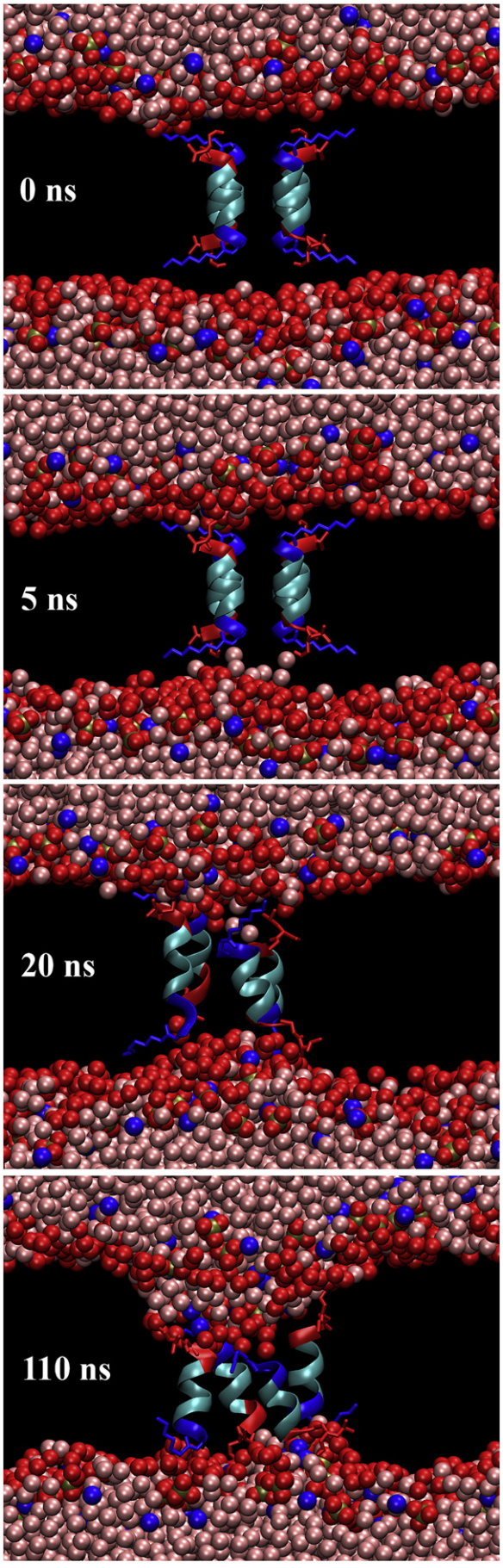

Fig. 4. Time evolution of a MD trajectory with 4 GAIV molecules embedded in the bilayer (including the 10 ns equilibration time). Phosphorus, nitrogen and oxygen atoms of phospholipids are shown as gold, blue and red spheres, respectively, while water oxygen atoms are colored in pink. The acyl chains of the phospholipids are omitted for the sake of clarity. Peptides are represented as ribbons, with the N- and C-termini are colored in blue and red, respectively. The *n*Oct and Lol moieties are shown in a "stick" representation. (For interpretation of the references to color in this figure legend, the reader is referred to the web version of this article.)

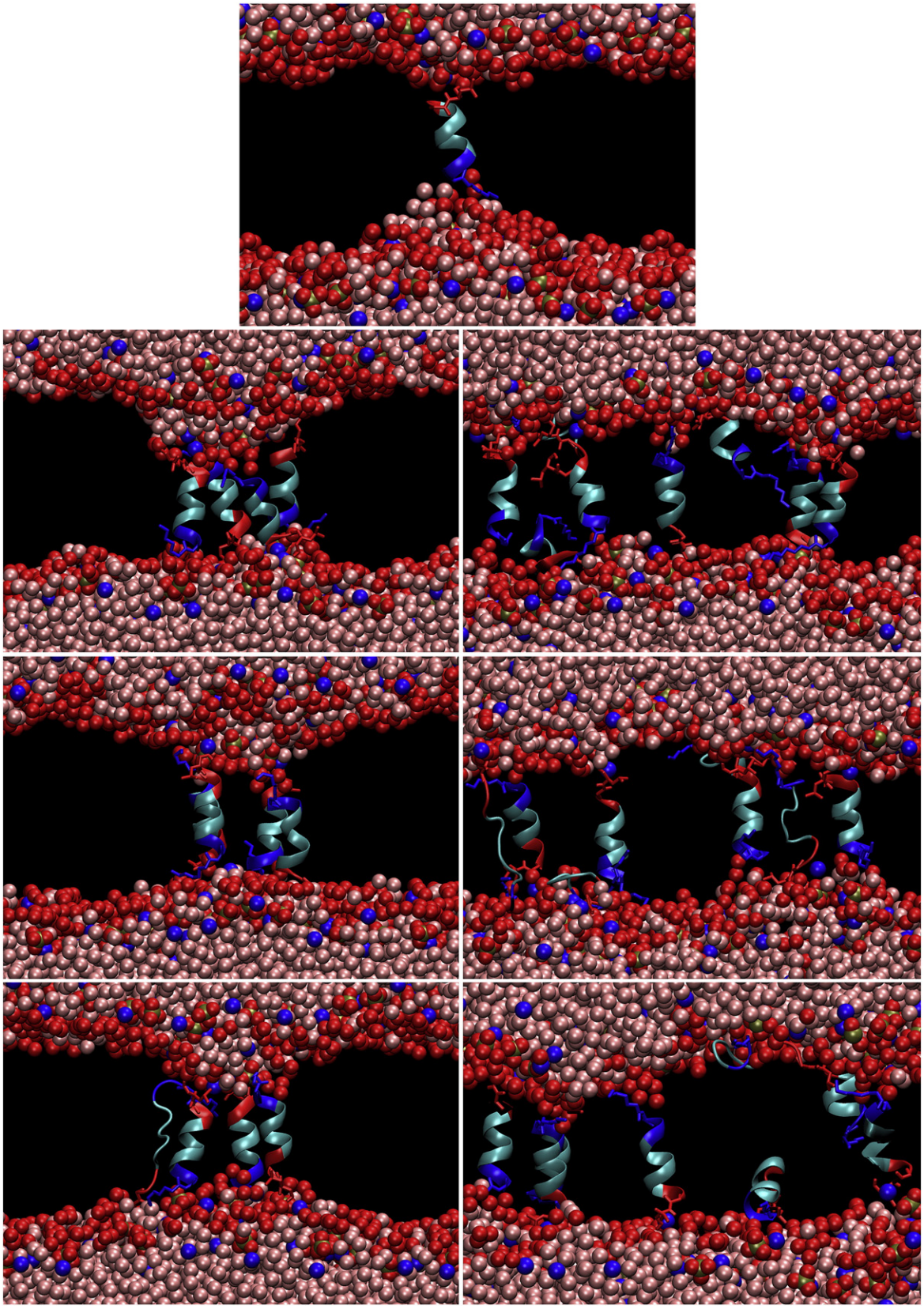

Fig. 5. Final structures in the simulations with 1, 4 or 8 GAIV molecules. The representations used are the same as those described in Fig. 3.

3.8. Comparison with the NR data

Neutron SLD profiles can be calculated from the MD trajectory and compared with the experimental data (Section 2). The SLD profiles calculated from the MD simulations, assuming a deuterated peptide and a hydrogenated membrane in heavy water are shown in Fig. S6. However, in order to perform a meaningful comparison, it was necessary to take into account the fact that in our experiments the lipid

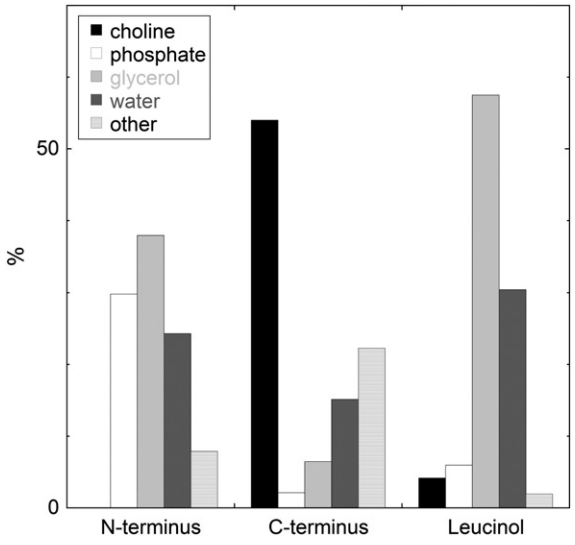

Fig. 6. Statistics of the interactions of selected peptide groups during the equilibrated segments of the MD trajectories with 4 GAIV molecules (30–110 ns). For each trajectory frame, the lipid or water atom closest to the different peptide groups (N-terminal NH, C-terminal CO and amino alcohol OH) was identified.

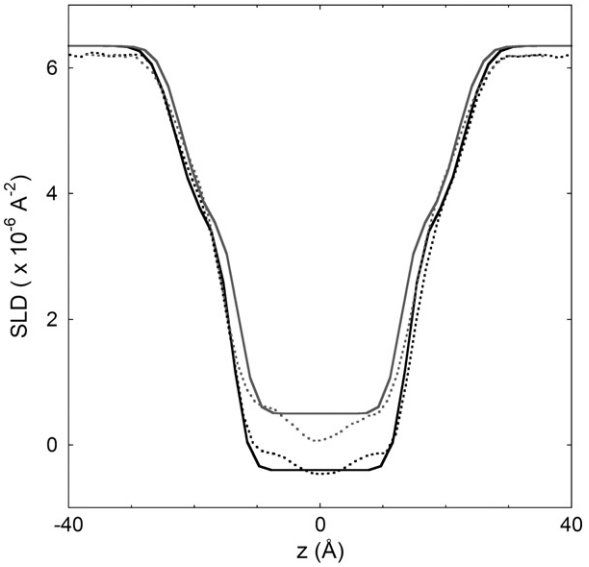

Fig. 7. Comparison between the neutron SLD profiles calculated from the MD trajectories of a peptide-free POPC bilayer (black dotted line) and in the presence of 8 GAIV molecules (gray dotted line, peptide to lipid ratio 0.0625) with the symmetrical profiles obtained from the experimental neutron data of the peptide-free bilayer (black solid line) and in the presence of deuterated GAIV at concentration C_1 (gray solid line, estimated inserted peptide to lipid ratio 0.07 ± 0.02; see Table 2).

bilayer was supported on a silicon crystal, while it was free-standing in water in the simulations. It was previously demonstrated that GAIV very quickly partitions in both layers of the membrane [35], and this should lead to a symmetrical SLD profile for a GAIV-containing bilayer in water. Therefore, the SLD profile of a free-standing membrane was obtained from the experimental profiles by reflecting the section of the profile corresponding to the water-facing side of the bilayer with respect to the center of the hydrophobic region. The comparison of the resulting profiles, reported in Fig. 7, shows a good qualitative agreement, regarding both the thickness of the bilayer and the increase in SLD due to GAIV insertion in the membrane. This comparison confers a good confidence to the atomic-level picture provided by the MD simulations.

3.9. Vesicle leakage experiments

Both the simulations and the neutron reflectivity experiments indicate the possibility for GAIV to span the bilayer entirely, by causing a significant thinning of the membrane. However, this bilayer deformation requires a free energy cost. Therefore, if a transmembrane orientation is involved in the GAIV pore-formation process, the membrane-perturbing activity of this peptide should increase significantly in thinner membranes, which require a smaller deformation or no thinning at all. To verify this point, we performed peptide-induced vesicle leakage experiments with liposomes formed by lipids with different chain lengths and bilayer thicknesses [73]. For comparison, the same experiments were carried out also with the much longer peptaibol Alm. As shown in Figs. 8 and 9, the activity of GAIV increases dramatically with decreasing the bilayer thickness, while that of Alm is affected only marginally. In bilayers with a thickness comparable to that of biological membranes, the activity of GAIV is much lower than that of Alm (Fig. 9). However, in the thinner membranes (whose hydrophobic core has a size comparable to that of the GAIV helix), the activity of the two peptides become comparable. It is also worth mentioning that the curves of peptide-induced leakage as a function of GAIV concentration (Fig. 8) are steeply sigmoidal in membranes with high thickness, indicating a strong cooperativity of the pore formation process, but this cooperativity decreases drastically in thinner membranes.

4. Discussion

Both our NR data and MD simulations show a GAIV-induced thinning of the membrane. The effect of the insertion of a peptide/protein in a bilayer with an equilibrium hydrophobic thickness differing from that of the inclusion has been rationalized in terms of hydrophobic mismatch [74,75]. The free energy cost of exposing to water hydrophobic groups of the protein or lipids, due to their different thickness, is higher than that of distorting the lipids from their equilibrium conformation. As a consequence, the membrane thickness locally adapts to the size of the inclusion, although other effects are also possible [76]. The case of GAIV falls under the category termed negative mismatch, where the inclusion is shorter than the membrane thickness. A systematic study on model peptides demonstrated that hydrophobic mismatch is sufficient to drive membrane thickness adjustments comparable to those that would be necessary for barrel-stave pore formation by GAIV [77]. However, our MD results indicate that, in the case of GAIV, membrane thinning might be driven also by specific interactions between the peptide N- and C-termini and the phospholipid headgroups. In this respect, it is important to note that we have previously shown that in solvents of low polarity GAIV binds cations with a very high affinity [39]. This result might reflect what is happening in the interaction between the peptide and lipid headgroups in the low dielectric environment of the bilayer core.

A completely different interpretation for peptide-induced membrane thinning has been provided by Huang [78], and used to describe the mechanism of action of both cationic AMPs and peptaibiotics. According to his model, binding of an amphipathic molecule to the bilayer surface at the water–lipid chain interface leads to an increase in the interfacial area, and thus to a decrease in the hydrocarbon thickness, due to the very low volume compressibility of the lipid chains. This deformation has an elastic energy penalty, and thus, at a threshold bound peptide concentration, a transmembrane orientation becomes favored. In this model, membrane thinning is due to the surface-bound peptide, rather than to the transmembrane-inserted molecules. Unfortunately, we have previously shown that in both orientations GAIV is located essentially in the hydrophobic core of the membrane [10,34,35] and therefore the NR data do not allow us to discriminate between the Huang hypothesis and thinning due to transmembrane inserted

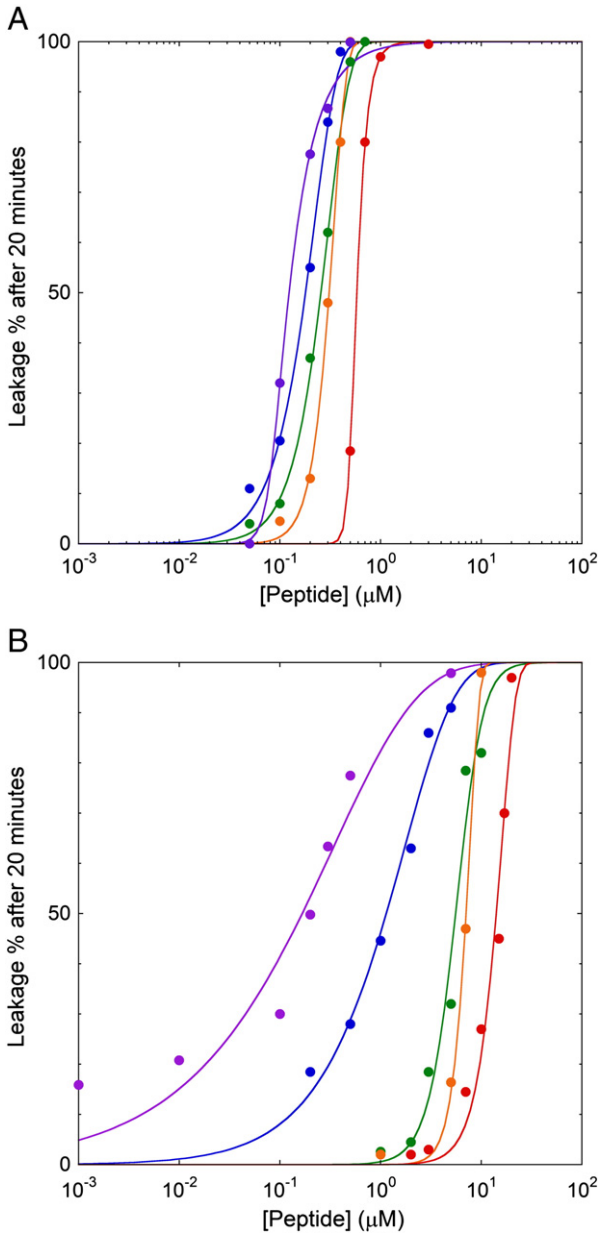

Fig. 8. Peptide-induced vesicle leakage 20 min after addition of different concentration of Alm (panel A) or GAIV (panel B), in bilayers of different thicknesses (lipid concentration 200 μM, vesicle diameter 200 nm). Red di22:1 PC (1,2-dierucoyl-*sn*-glycero-3-phosphocholine); orange di20:1 PC (1,2-dieicosenoyl-*sn*-glycero-3-phosphocholine); green di18:1 PC (1,2-dioleoyl-*sn*-glycero-3-phosphocholine); blue di16:1 PC (1,2-dipalmitoleoyl-*sn*-glycero-3-phosphocholine); and violet di14:1 PC (1,2-dimyristoleoyl-*sn*-glycero-3-phosphocholine). (For interpretation of the references to color in this figure legend, the reader is referred to the web version of this article.)

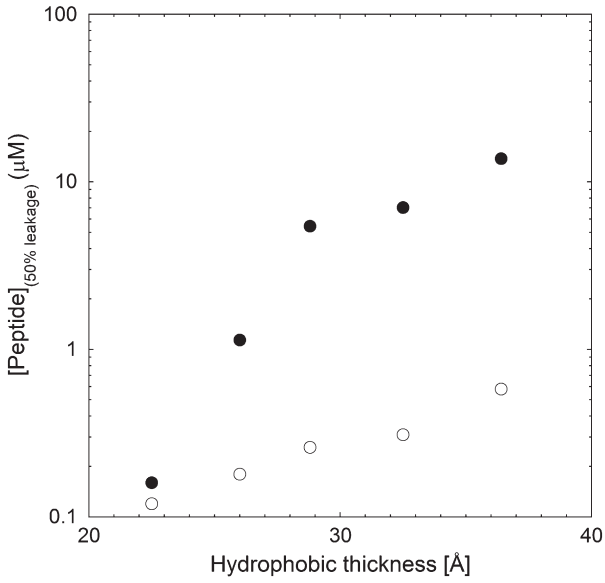

Fig. 9. Membrane-permeabilizing peptide activity as a function of the hydrophobic thickness of the bilayer [69]. The peptide concentration required to induce the leakage of 50% of liposome contents (lipid concentration 200 μM, vesicle diameter 200 nm) in 20 min was calculated from the leakage curves reported in Fig. 8, and is shown for Alm (empty symbols) and GAIV (solid symbols).

peptides. However, several indications suggest that the Huang mechanism is unlikely for GAIV: insertion of this highly hydrophobic peptide in the phospholipid tail region, parallel to the membrane surface, can be easily accommodated, without causing a significant increase in the interfacial area nor a perturbation of membrane order, as also shown by previous simulations and experiments performed by our group [10].

Whatever the driving force of the GAIV-induced membrane thinning might be, this effect makes possible for the peptide to span the bilayer from one side to the other, and also provides a rationalization to a series of experimental observations regarding this peptaibol. Our fluorescence experiments demonstrated that membrane-inserted GAIV exists essentially in an aggregate state [34,35]. Clearly, the free energy cost of membrane deformation can be significantly reduced by peptide aggregation (just like in the hydrophobic effect aggregation of apolar molecules in water reduces the entropic cost of water structuring around them). Therefore, a monomeric transmembrane mismatched inclusion is significantly unstable [76]. This is probably the main driving force for the highly cooperative GAIV oligomerization in membrane-permeabilizing channels. This interpretation would also explain the observation that curves of membrane-perturbing activity as a function of GAIV concentration are highly cooperative in thick membranes, while this cooperativity decreases significantly in thinner membranes (Fig. 8). The strong dependence of GAIV activity on membrane thickness observed here is another evidence which can be easily explained as due to the degree of membrane thinning necessary for this peptide to span the whole bilayer. The observation that, on the other hand, Alm activity is not very sensitive to the thickness of the bilayer is consistent with previous studies on model peptides, which show that long peptides can easily adapt to insertion in a thinner membrane by tilting [79]. In principle, a large difference in GAIV activity between thin and thick membranes could be also due to a transition from a barrel-stave pore formed by a single GAIV layer to a “double barrel” of trichogin dimers [27,32]. However, the membrane thinning observed in the NR experiments is an indication contrasting this interpretation, at least in the POPC bilayers used in those measurements, which have a thickness comparable to natural membranes.

Alm is one of the longest peptaibiotics, but many “medium”- or “short”-length peptides of this class do exist [11,80]. Therefore, the present findings might be relevant for a rather wide class of peptides. Longer peptaibols are much more active than shorter ones [81], but barrel-stave channel formation has been hypothesized for some of the latter, like the 16 residue long antiamoebin [82]. Solid-state NMR measurements have also shown that such relatively short peptides, like the 14 residue ampullosporin or the 15 residue zervamicin II, attain a predominantly transmembrane orientation when the membrane thickness is comparable to their length, while they are largely parallel to the surface in thicker bilayers [83,84]. Therefore, it has been proposed that all peptaibiotics might act according to the barrel-stave mechanism, the lower activity of the shorter ones being due to the lowest fraction of peptide molecules in a transmembrane orientation [84].

Some other findings reported in the literature further support the possibility for a peptaibiotic to form barrel-stave channels in a membrane thicker than its length. For instance, Alm is able to form pores even in artificial membranes formed by diblock copolymers whose hydrophobic region is much thicker than the peptide length [85], thus paralleling the situation of GAIV in biological membranes. In addition, our findings regarding the membrane thickness dependence of GAIV activity nicely parallel the observation that in a series of short-chain GAIV analogs the activity significantly and progressively decreased with the shortening of the peptide chain [86].

No electrophysiology measurements of the conductance of single GAIV channels in planar membranes, which would provide a conclusive confirmation of a barrel-stave mechanism, have been reported to date. However, experiments on liposomes have shown that the pores formed by this peptide are ion selective and that their conductance is voltage-dependent, as it would be expected for Alm-like barrel-stave pores [44]. The voltage-gated nature of the GAIV channels was recently confirmed also by electrochemical measurements on Hg-supported tethered bilayer lipid membranes [42].

Overall, the present data indicate that formation of transmembrane barrel-stave channels might indeed be possible even for short peptaibiotics.

Acknowledgements

The authors wish to thank the Institut Laue-Langevin in Grenoble (FR), and ISIS for beam-time and use of laboratory facilities. Financial support by the Italian Ministry of Education, University and Research (PRIN project, grant 2008), CNR (agreement no. 01/9001), CINECA (grant HP10CA881J), the Italian Ministry of Foreign Affairs, CASPUR (grant std12-138), and the Fermi Research Center is gratefully acknowledged.

Appendix A. Supplementary data

Supplementary data to this article can be found online at http://dx.doi.org/10.1016/j.bbamem.2012.11.033.

References

[1] A.T. Yeung, S.L. Gellatly, R.E.W. Hancock, Multifunctional cationic host defence peptides and their clinical applications, Cell. Mol. Life Sci. 68 (2011) 2161–2176.
[2] W.C. Wimley, Describing the mechanism of antimicrobial peptide action with the interfacial activity model, ACS Chem. Biol. 5 (2010) 905–917.
[3] L. Zhang, T.J. Falla, Potential therapeutic application of host defense peptides, in: A. Giuliani, A.C. Rinaldi (Eds.), Antimicrobial Peptides, Methods in Molecular Biology, 618, Springer, 2010, pp. 303–327.
[4] N.K. Brogden, K.A. Brogden, Will new generations of modified antimicrobial peptides improve their potential as pharmaceuticals? Int. J. Antimicrob. Agents 38 (2011) 217–225.
[5] C.D. Fjell, J.A. Hiss, R.E.W. Hancock, G. Schneider, Designing antimicrobial peptides: form follows function, Nat. Rev. Drug Discov. 11 (2012) 37–51.
[6] D. Takahashi, S.K. Shukla, O. Prakash, G. Zhang, Structural determinants of host defense peptides for antimicrobial activity and target cell selectivity, Biochimie 92 (2010) 1236–1241.
[7] E. Gazit, I.R. Miller, P.C. Biggin, M.S. Sansom, Y. Shai, Structure and orientation of the mammalian antibacterial peptide cecropin P1 within phospholipid membranes, J. Mol. Biol. 258 (1996) 860–870.
[8] K. Matsuzaki, O. Murase, H. Tokuda, S. Funakoshi, N. Fujii, K. Miyajima, Orientational and aggregational states of magainin2 in phospholipid bilayers, Biochemistry 33 (1994) 3342–3349.
[9] S.J. Ludtke, K. He, W.T. Heller, T.A. Harroun, L. Yang, H.W. Huang, Membrane pores induced by magainin, Biochemistry 35 (1996) 13,723–13,728.
[10] G. Bocchinfuso, A. Palleschi, B. Orioni, G. Grande, F. Formaggio, C. Toniolo, Y. Park, K.S. Hahm, L. Stella, Different mechanisms of action of antimicrobial peptides: insights from fluorescence spectroscopy experiments and molecular dynamics simulations, J. Pept. Sci. 15 (2009) 550–558.
[11] In: C. Toniolo, H. Brückner (Eds.), Peptaibiotics, Wiley-VCH, 2009.
[12] B. Leitgeb, A. Szekeres, L. Manczinger, C. Vágvölgyi, L. Kredics, The history of alamethicin: a review of the most extensively studied peptaibol, Chem. Biodivers. 4 (2007) 1027–1051.
[13] G. Baumann, P. Mueller, A molecular model of membrane excitability, J. Supramol. Struct. 2 (1974) 538–557.
[14] G. Boheim, Statistical analysis of alamethicin channels in black lipid membranes, J. Membr. Biol. 19 (1974) 277–303.
[15] R.O. Fox, F.M. Richards, A voltage-gated ion channel model inferred from the crystal structure of alamethicin at 1.5 Å resolution, Nature 300 (1982) 325–330.
[16] D.S. Cafiso, Alamethicin: a peptide model for voltage gating and protein–membrane interactions, Annu. Rev. Biophys. Biomol. Struct. 23 (1994) 141–165.
[17] D.R. Laver, The barrel-stave model as applied to alamethicin and its analogs reevaluated, Biophys. J. 66 (1994) 355–359.
[18] H. Duclohier, H. Wróblewski, Voltage-dependent pore formation and antimicrobial activity by alamethicin and analogues, J. Membr. Biol. 184 (2001) 1–12.
[19] L. Stella, M. Burattini, C. Mazzuca, A. Palleschi, M. Venanzi, C. Baldini, F. Formaggio, C. Toniolo, B. Pispisa, Alamethicin interaction with lipid membranes: a spectroscopic study on synthetic analogues, Chem. Biodivers. 4 (2007) 1299–1312.
[20] S. Ye, H. Li, F. Wei, J. Jasensky, A.P. Boughton, P. Yang, Z. Chen, Observing a model ion channel gating action in model cell membranes in real time in situ: membrane potential change induced alamethicin orientation change, J. Am. Chem. Soc. 134 (2012) 6237–6243.
[21] B. Bechinger, A dynamic view of peptides and proteins in membranes, Cell. Mol. Life Sci. 65 (2008) 3028–3039.
[22] E. Salnikov, C. Aisenbrey, V. Vidovic, B. Bechinger, Solid-state NMR approaches to measure topological equilibria and dynamics of membrane polypeptides, Biochim. Biophys. Acta 1798 (2010) 258–265.
[23] M. De Zotti, B. Biondi, F. Formaggio, C. Toniolo, L. Stella, Y. Park, K.-S. Hahm, Trichogin GA IV: an antibacterial and protease-resistant peptide, J. Pept. Sci. 15 (2009) 615–619.
[24] C. Auvin-Guette, S. Rebuffat, Y. Prigent, B. Bodo, Trichogin A IV, an 11-residue lipopeptaibol from *Trichoderma longibrachiatum*, J. Am. Chem. Soc. 114 (1992) 2170–2172.
[25] C. Peggion, F. Formaggio, M. Crisma, R.F. Epand, R.M. Epand, C. Toniolo, Trichogin: a paradigm for lipopeptaibols, J. Pept. Sci. 9 (2003) 679–689.
[26] C. Heuber, F. Formaggio, C. Baldini, C. Toniolo, K. Müller, Multinuclear solid-state-NMR and FT-IR-absorption investigations on lipid/trichogin bilayers, Chem. Biodivers. 4 (2007) 1200–1218.
[27] C. Toniolo, C. Peggion, M. Crisma, F. Formaggio, X. Shui, D.S. Eggleston, Structure determination of racemic trigogin A IV using centrosymmetric crystals, Nat. Struct. Biol. 1 (1994) 908–914.
[28] V. Monaco, F. Formaggio, M. Crisma, C. Toniolo, P. Hanson, G.L. Millhauser, Orientation and immersion depth of a helical lipopeptaibol in membranes using TOAC as an ESR probe, Biopolymers 50 (1999) 239–253.
[29] A.D. Milov, Yu.D. Tsvetkov, F. Formaggio, M. Crisma, C. Toniolo, J. Raap, Self-assembling properties of membrane-modifying peptides studied by PELDOR and CW-ESR spectroscopies, J. Am. Chem. Soc. 122 (2000) 3843–3848.
[30] A.D. Milov, Y.D. Tsvetkov, F. Formaggio, M. Crisma, C. Toniolo, J. Raap, Self-assembling and membrane modifying properties of a lipopeptaibol studied by CW-ESR and PELDOR spectroscopies, J. Pept. Sci. 9 (2003) 690–700.
[31] E.S. Salnikov, D.A. Erilov, A.D. Milov, Y.D. Tsvetkov, C. Peggion, F. Formaggio, C. Toniolo, J. Raap, S.A. Dzuba, Location and aggregation of the spin-labeled peptide trichogin GA IV in a phospholipid membrane as revealed by pulsed EPR, Biophys. J. 91 (2006) 1532–1540.
[32] V.N. Syryamina, N.P. Isaev, C. Peggion, F. Formaggio, C. Toniolo, J. Raap, S.A. Dzuba, Small-amplitude backbone motions of the spin-labeled lipopeptide trichogin GA IV in a lipid membrane as revealed by electron spin echo, J. Phys. Chem. B 114 (2010) 12,277–12,283.
[33] V.N. Syryamina, M. De Zotti, C. Peggion, F. Formaggio, C. Toniolo, J. Raap, S.A. Dzuba, A molecular view on the role of cholesterol upon membrane insertion, aggregation, and water accessibility of the antibiotic lipopeptide trichogin GA IV as revealed by EPR, J. Phys. Chem. B 116 (2012) 5653–5660.
[34] L. Stella, C. Mazzuca, M. Venanzi, A. Palleschi, M. Didonè, F. Formaggio, C. Toniolo, B. Pispisa, Aggregation and water-membrane partition as major determinants of the activity of the antibiotic peptide trichogin GA IV, Biophys. J. 86 (2004) 936–945.
[35] C. Mazzuca, L. Stella, M. Venanzi, F. Formaggio, C. Toniolo, B. Pispisa, Mechanism of membrane activity of the antibiotic trichogin GA IV: a two-state transition controlled by peptide concentration, Biophys. J. 88 (2005) 3411–3421.
[36] E. Gatto, C. Mazzuca, L. Stella, M. Venanzi, C. Toniolo, B. Pispisa, Effect of peptide lipidation on membrane perturbing activity: a comparative study on two trichogin analogues, J. Phys. Chem. B 110 (2006) 22,813–22,818.
[37] M. Venanzi, E. Gatto, G. Bocchinfuso, A. Palleschi, L. Stella, C. Baldini, F. Formaggio, C. Toniolo, Peptide folding dynamics: a time-resolved study from the nanosecond to the microsecond time regime, J. Phys. Chem. B 110 (2006) 22,834–22,841.
[38] M. Venanzi, E. Gatto, G. Bocchinfuso, A. Palleschi, L. Stella, F. Formaggio, C. Toniolo, Dynamics of formation of a helix–turn–helix structure in a membrane-active peptide: a time-resolved spectroscopic study, Chembiochem 7 (2006) 43–45.
[39] M. Venanzi, G. Bocchinfuso, E. Gatto, A. Palleschi, L. Stella, F. Formaggio, C. Toniolo, Metal binding properties of fluorescent analogues of trichogin GA IV: a conformational study by time-resolved spectroscopy and molecular mechanics investigations, Chembiochem 10 (2009) 91–97.
[40] C. Mazzuca, B. Orioni, M. Coletta, F. Formaggio, C. Toniolo, G. Maulucci, M. De Spirito, B. Pispisa, M. Venanzi, L. Stella, Fluctuations and the rate-limiting step of peptide-induced membrane leakage, Biophys. J. 99 (2010) 1791–1800.
[41] S. Smeazzetto, M. De Zotti, M.R. Moncelli, A new approach to detect and study ion channel formation in microBLMs, Electrochem. Commun. 13 (2011) 834–836.
[42] L. Becucci, F. Maran, R. Guidelli, Probing membrane permeabilization by the antibiotic lipopeptaibol trichogin GA IV in a tethered bilayer lipid membrane, Biochim. Biophys. Acta 1818 (2012) 1656–1662.

[43] R.F. Epand, R.M. Epand, V. Monaco, S. Stoia, F. Formaggio, M. Crisma, C. Toniolo, The antimicrobial peptide trichogin and its interaction with phospholipid membranes, Eur. J. Biochem. 266 (1999) 1021–1028.
[44] T.N. Kropacheva, J. Raap, Ion transport across a phospholipid membrane mediated by the peptide trichogin GA IV, Biochim. Biophys. Acta 1567 (2002) 193–203.
[45] P.J. Bond, M.S.P. Sansom, Insertion and assembly of membrane proteins via simulation, J. Am. Chem. Soc. 128 (2006) 2697–2704.
[46] S. Esteban-Martin, J. Salgado, Self-assembling of peptide/membrane complexes by atomistic molecular dynamics simulations, Biophys. J. 92 (2007) 903–912.
[47] B. Orioni, G. Bocchinfuso, J.Y. Kim, A. Palleschi, G. Grande, S. Bobone, Y. Park, J.I. Kim, K.S. Hahm, L. Stella, Membrane perturbation by the antimicrobial peptide PMAP-23: a fluorescence and molecular dynamics study, Biochim. Biophys. Acta 1788 (2009) 1523–1533.
[48] G. Bocchinfuso, S. Bobone, A. Palleschi, L. Stella, Fluorescence spectroscopy and molecular dynamics simulations in studies on the mechanism of membrane destabilization by antimicrobial peptides, Cell. Mol. Life Sci. 68 (2011) 2281–2301.
[49] M. De Zotti, B. Biondi, C. Peggion, F. Formaggio, Y. Park, K.-S. Hahm, C. Toniolo, Trichogin GA IV: a versatile template for the synthesis of novel peptaibiotics, Org. Biomol. Chem. 10 (2012) 1285–1299.
[50] T. Crowley, E. Lee, E. Simister, R. Thomas, The use of contrast variation in the specular reflection of neutrons from interfaces, Physica B 173 (1991) 143–156.
[51] R. Cubitt, G. Fragneto, D17: the new reflectometer at the ILL, Appl. Phys. A: Mater. Sci. Process. 74 (2002) s329–s331.
[52] V. Sears, Neutron scattering lengths and cross sections, Neutron News 3 (1992) 26–37.
[53] E. Kalb, S. Frey, L.K. Tamm, Formation of supported planar bilayers by fusion of vesicles to supported phospholipid monolayers, Biochim. Biophys. Acta 1103 (1992) 307–316.
[54] J. Penfold, R. Thomas, The application of the specular reflection of neutrons to the study of surfaces and interfaces, J. Phys. Condens. Matter 2 (1990) 1369.
[55] L.G. Parratt, Surface studies of solids by total reflection of X-rays, Phys. Rev. 95 (1954) 359–369.
[56] F. James, MINUIT Minimization Package, Reference Manual, CERN Program Library, Geneva, 1994.
[57] D.P. Tieleman, J. Breed, H.J. Berendsen, M.S. Sansom, Alamethicin channels in a membrane: molecular dynamics simulations, Faraday Discuss. 111 (1998) 209–223.
[58] W.F. van Gunsteren, H.J.C. Berendsen, Groningen molecular simulation (GROMOS) library manual, BIOMOS b.v., Groningen (The Netherlands), 1987.
[59] B. Hess, C. Kutzner, D. van der Spoel, E. Lindahl, GROMACS 4: algorithms for highly efficient, load-balanced, and scalable molecular simulation, J. Chem. Theory Comput. 4 (2008) 435–447.
[60] D. van der Spoel, E. Lindahl, B. Hess, A.R. van Buuren, E. Apol, P.J. Meulenhoff, D.P. Tieleman, A.L.T.M. Sijbers, K.A. Feenstra, R. van Drunen, H.J.C. Berendsen, Gromacs User Manual Version 4.5.4, www.gromacs.org2010.
[61] H.J.C. Berendsen, J.P.M. Postma, W.F. van Gunsteren, A. Di Nola, J.R. Haak, Molecular dynamics with coupling to an external bath, J. Chem. Phys. 81 (1984) 3684–3690.
[62] W. Humphrey, A. Dalke, K. Shulten, VMD: visual molecular dynamics, J. Mol. Graph. 14 (1996) 33–38.
[63] N. Kučerka, S. Tristram-Nagle, J.F. Nagle, Structure of fully hydrated fluid phase lipid bilayers with monounsaturated chains, J. Membr. Biol. 208 (2005) 193–202.
[64] J. Daillant, Structure and fluctuations of a single floating lipid bilayer, Proc. Natl. Acad. Sci. U. S. A. 102 (2005) 11,639–11,644.
[65] T.B. Woolf, B. Roux, Structure, energetics, and dynamics of lipid–protein interactions: a molecular dynamics study of the gramicidin a channel in a DMPC bilayer, Proteins 24 (1996) 92–114.
[66] S. Jo, T. Kim, W. Im, Automated builder and database of protein/membrane complexes for molecular dynamics simulations, PLoS One (2007) e880.
[67] D.P. Tieleman, Methods and parameters for membrane simulations, in: M.S.P. Sansom, P.C. Biggin (Eds.), Molecular Simulations and Biomembranes: From Biophysics to Function, RSC, 2010, pp. 1–25.
[68] D.P. Tieleman, H.J.C. Berendsen, M.S.P. Sansom, An alamethicin channel in a lipid bilayer: molecular dynamics simulations, Biophys. J. 76 (1999) 1757–1769.
[69] M.G. Wolf, M. Hoefling, C. Aponte-Santamaría, H. Grubmüller, G. Groenhof, g_membed: efficient insertion of a membrane protein into an equilibrated lipid bilayer with minimal perturbation, J. Comput. Chem. 31 (2010) 2169–2174.
[70] J. Faraldo-Gómez, G. Smith, M. Sansom, Setting up and optimization of membrane protein simulations, Eur. Biophys. J. 31 (2002) 217–227.
[71] R. Staritzbichler, C. Anselmi, L.R. Forrest, J.D. Faraldo-Gómez, GRIFFIN: a versatile methodology for optimization of protein–lipid interfaces for membrane protein simulations, J. Chem. Theory Comput. 7 (2011) 1167–1176.
[72] C. Kandt, W.L. Ash, D.P. Tieleman, Setting up and running molecular dynamics simulations of membrane proteins, Methods 41 (2007) 475–488.
[73] A. Hinderliter, R.L. Biltonen, P.F.F. Almeida, Lipid modulation of protein-induced membrane domains as a mechanism for controlling signal transduction, Biochemistry 43 (2004) 7102–7110.
[74] O.G. Mouritsen, M. Bloom, Mattress model of lipid–protein interactions in membranes, Biophys. J. 46 (1984) 141–153.
[75] J.A. Killian, Hydrophobic mismatch between proteins and lipids in membranes, Biochim. Biophys. Acta 1376 (1998) 401–416.
[76] J.A. Killian, T.K.M. Nyholm, Peptides in lipid bilayers: the power of simple models, Curr. Opin. Struct. Biol. 16 (2006) 473–479.
[77] S.S. Krishnakumar, E. London, Effect of sequence hydrophobicity and bilayer width upon the minimum length required for the formation of transmembrane helices in membranes, J. Mol. Biol. 374 (2007) 671–687.
[78] H.W. Huang, Free energies of molecular bound states in lipid bilayers: lethal concentrations of antimicrobial peptides, Biophy. J. 96 (2009) 3263–3272.
[79] U. Harzer, B. Bechinger, Alignment of lysine-anchored membrane peptides under conditions of hydrophobic mismatch: a CD, ^{15}N and ^{31}P solid-state NMR spectroscopy investigation, Biochemistry 39 (2000) 13,106–13,114.
[80] T. Degenkolb, J. Kirschbaum, H. Brückner, New sequences, constituents and producers of peptaibiotics: an updated review, Chem. Biodivers. 4 (2007) 1052–1067.
[81] P.A. Grigoriev, B. Schlegel, M. Kronen, A. Berg, A. Härtl, U. Gräfe, Differences in membrane pore formation by peptaibols, J. Pept. Sci. 9 (2003) 763–768.
[82] H. Duclohier, C.F. Snook, B.A. Wallace, Antiamoebin can function as a carrier or as a pore-forming peptaibol, Biochim. Biophys. Acta 1415 (1998) 255–260.
[83] B. Bechinger, D.A. Skladnev, A. Ogrel, X. Li, E.V. Rogozhkina, T.V. Ovchinnikova, J.D.J. O'Neil, J. Raap, ^{15}N and ^{31}P solid-state NMR investigations on the orientation of zervamicin II and alamethicin in phosphatidylcholine membranes, Biochemistry 40 (2001) 9428–9437.
[84] E.S. Salnikov, H. Friedrich, X. Li, P. Bertani, S. Reissmann, C. Hertweck, J.D.J. O'Neil, J. Raap, B. Bechinger, Structure and alignment of the membrane-associated peptaibols ampullosporin A and alamethicin by oriented ^{15}N and ^{31}P solid-state NMR spectroscopy, Biophys. J. 96 (2009) 86–100.
[85] K. Vijayan, D.E. Discher, J. Lal, P. Janmey, M. Goulian, Interactions of membrane-active peptides with thick, neutral, nonzwitterionic bilayers, J. Phys. Chem. B 109 (2005) 14,356–14,364.
[86] F. Formaggio, C. Peggion, M. Crisma, C. Toniolo, Short-chain analogues of the lipopeptaibol antibiotic trichogin GA IV: conformational analysis and membrane modifying properties, J. Chem. Soc., Perkin Trans. 2 (2001) 1372–1377.